Controlled Structure of Gallium Oxide Nanowires

Hye Jin Chun and Young Sang Choi

Department of Chemistry, Korea University, 1 Anam Seoul 136-701, South Korea

Seung Yong Bae, Hee Won Seo, Su Jin Hong, and Jeunghee Park*

Department of Chemistry, Korea University, Jochiwon 339−700, South Korea

Hyunik Yang

College of Engineering Science, Hanyang University, Ansan 425−791, South Korea

Received: March 21, 2003; In Final Form: May 21, 2003

Gallium oxide nanowires were synthesized via chemical vapor deposition of gallium/gallium oxide mixture and oxygen. The diameter of the nanowires is 30−80 nm with an average value of 50 nm. They consist of single-crystalline monoclinic crystal. While the nanowires grown without catalyst exhibit a significant planar defect, the nanowires grown with nickel catalytic nanopaticles are almost defect-free. The growth direction of the nanowires grown without the catalyst is uniformly [010]. In contrast, the nanowires grown with the catalyst have random growth direction. X-ray diffraction, Raman spectroscopy, and photoluminescence are well correlated with the structural characteristics of the nanowires. The result provides an evidence for the catalyst effect in controlling the structure of nanowires.

1. Introduction

Monoclinic gallium oxide (β-Ga_2O_3) is an important wide band gap (E_g = 4.9 eV at 300 K) material because of good chemical and thermal stability. It has a variety of applications including transparent conducting oxide,[1−4] optical emitter for UV,[5] and gas sensors.[6,7] Their nanostructures such as nanowires, nanobelts, and nanosheets are currently the subject of intense research because of the potential for nanoscale electronic and optoelectronic applications. They are expected to exhibit unique physical properties, distinctive from those of the bulk materials. The synthesis and characterization of β-Ga_2O_3 nanostructures have been lately progressed. Various methods, for example, arc discharge,[8,9] laser ablation,[10] thermal oxidation,[11−17] and carbothermal reduction,[18−23] were developed by several research groups. The β-Ga_2O_3 nanowires were prepared by arc discharge of GaN[8,9] and a laser ablation of Ga_2O_3 target using 248 nm.[10] Ga,[11−14] GaAs,[15] and GaN[16,17] were thermally oxidized to synthesize various forms of nanostructure. The carbothermal reduction of Ga_2O_3 powder using carbon produced the β-Ga_2O_3 nanowires and nanobelts.[18−22] Recently, the β-Ga_2O_3 nanowires sheathed with boron nitride layers were synthesized by reacting Ga_2O_3 powder with amorphous boron.[23] However, despite the tremendous amount of syntheses, the control of the structure has not been much achieved yet.

In this paper, we report a simple and large-scale synthesis of β-Ga_2O_3 nanowires by a thermal chemical vapor deposition using the oxidation of Ga/Ga_2O_3 mixture. We observed that the structure of the nanowires could be controlled by the use of catalyst. The morphology, the degree of crystalline perfection, and the growth direction depending on the growth condition were examined by scanning electron microscopy (SEM), transmission electron microscopy (TEM), electron diffraction (ED), X-ray diffraction (XRD), Raman spectroscopy, and photoluminescence (PL).

2. Experimental Section

Ga (99.999%, Aldrich) and Ga_2O_3 (99.999%, Aldrich) with a molar ratio of 4:1 were placed in a quartz boat located inside a quartz tube reactor. The alumina substrates were coated with 0.01 M ethanol solution of $NiCl_2 \cdot 6H_2O$ (99.99%, Aldrich), leading the deposition of Ni catalytic nanoparticles. The uncoated substrates or coated substrates were placed on the quartz boat. The temperature of the reactor was set at 1000−1200 °C. Ar flowed constantly at a rate of 500 standard cubic centimeters per minute (sccm). The growth time was 30 min to 1 h. When the uncoated substrates were used, the O_2/Ar flow (2−10/500 sccm) was maintained during the growth to maximize the yield of nanowires. A white-colored, wool-like product was deposited as a thick film on the alumina substrate. The size and structure of the product were examined using SEM (Hitachi S-4300), TEM (JEOL JEM-2010, 200 kV), ED, energy-dispersive X-ray spectroscopy (EDS), powder XRD (Philips X'PERT MPD), and Raman spectroscopy (Renishaw 1000) using a 514.5-nm argon ion laser. PL was conducted at room temperature with the 325-nm line from a helium−cadmium (He−Cd) laser. The laser power was about 1 kW/cm^2.

3. Results and Discussion

SEM image reveals that the product is high-density nanowires grown without catalyst (Figure 1a). Let us denote the product as NWs-1. The length of nanowires is 10−20 μm. The nanowires are grown with a negligible amount of nanoparticle impurities or other nanostructures. Magnified SEM images show that the surface of the nanowires is clean and the cross section is usually not round (Figure 1b and its inset). The EDS analysis

* Corresponding author. E-mail: parkjh@korea.ac.kr.

10.1021/jp034728o CCC: $25.00
Published on Web 07/12/2003

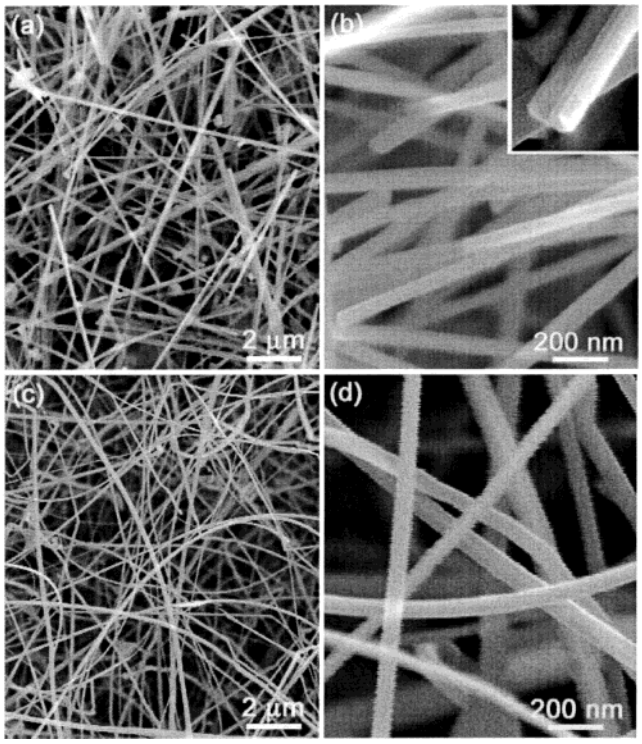

Figure 1. (a) SEM micrograph of the β-Ga_2O_3 nanowires grown without catalyst. (b) A magnified image reveals the clean surface and the angled cross section (inset). (c) SEM micrograph of the β-Ga_2O_3 nanowires grown with the Ni catalyst. (b) A magnified image shows the high purity of Ga_2O_3 nanowires.

identifies only Ga and O components. Further structure analyses below confirm that these wirelike materials are indeed composed of β-Ga_2O_3 crystal. When the Ni catalyst-deposited alumina substrate is used, the flow of O_2 was unnecessary to achieve a high density of the nanowires. Parts c and d of Figure 1 show the nanowires grown on the substrate. Let us denote these nanowires grown with the Ni catalyst as NWs-2. They are grown without any nanoparticle impurities or other nanostructures. The length of nanowires is up to 500 μm, which is much longer than NWs-1. They appear to be more flexible than NWs-1. Magnified view reveals the clean surface of the nanowires without any nanoparticles. The cross section of the nanowires is almost round, which is distinguished from NWs-1.

Figure 2 shows the TEM images of NWs-1. All nanowires are straight and smooth in surface (Figure 2a). The diameter of nanowires is 40−70 nm with an average value of 50 nm. There are few amorphous outerlayers (Figure 2b). The end of the nanowires is not flat but rather sharp. Figure 2c shows HRTEM image for a single-crystalline β-Ga_2O_3 nanowire. The [010] direction of monoclinic unit cell is aligned to the wire axis (growth direction). The dark lines along the growth direction would result from the defects such as stacking fault. The selected-areas ED (SAED) pattern taken from the <001> zone axis further confirms the single-crystalline structure, the [010] growth direction, and a significant defect perpendicular the growth direction (inset). Figure 2d shows the (200) fringes parallel to the wire axis that are separated by about 5.94 Å, which is consistent with that of bulk β-Ga_2O_3 crystal (a = 12.227 Å, b = 3.0389 Å, c = 5.8079 Å, β = 103.7°; JCPDS Card No. 41-1103). Figure 2e corresponds to the HRTEM image of another nanowire having a sharp tip. The strong dark lines near the center indicate a significant stacking fault. The SAED pattern shows the [010] growth direction and the stacking faults perpendicular to the growth direction (inset). Atomic-resolved image for the tip part reveal that the distance between neighboring (200) planes becomes short near the centerline of the nanowire, corresponding to a planar defect perpendicular to the growth direction (Figure 2f). All of the nanowires, we observed, are grown uniformly with the [010] growth direction. Most of them contain significant planar defects in the proximity of the centerline.

Figure 3 shows the TEM images for the NWs-2. The diameter of nanowires is 30−80 nm with an average value of 50 nm that is about the same as that of NWs-1 (Figure 3a). They are longer and more flexible compared to NWs-1. No amorphous outerlayers are observed from the nanowires (Figure 3b). The side edges show frequently a steplike morphology. No catalytic particles attach at the end of the nanowires. The HRTEM image of individual nanowire reveals its steplike side edges (Figure 3c). The nanowire consists of a single-crystalline β-Ga_2O_3 crystal that the [200] direction is perpendicular to the wire axis. The SAED pattern further confirms the single-crystalline structure with negligible defects (inset). The angle between the growth direction and the [001] direction is about 13°. Figure 3d shows the (200) fringes parallel to the wire axis that are separated by about 5.94 Å. Figure 3e shows an HRTEM image and its SAED pattern of another nanowire whose growth direction is tilted to the $[\bar{2}0\bar{2}]$ direction with an angle of 15°. Atomic-resolved image reveals well-separated (111) planes with a distance of 2.51 Å (Figure 3f). We observed that the nanowires grown with the Ni catalyst have a variety of growth directions and nearly defect-free crystalline structure.

The XRD patterns for the nanowires (NWs-1 and NWs-2) detached from the substrate are displayed in Figure 4 with that of the commercially available β-Ga_2O_3 powder (99.999%, Aldrich). The peaks can be indexed to the β-Ga_2O_3 crystal. The position of each peak is nearly the same for three samples. No other crystalline forms are detected from the nanowire samples. In the powder, the (002) and (111) peaks exhibit a high intensity, which is consistent with the reported pattern (JCPDS Card No. 41-1103). For the nanowires, the relative peak intensity could be directly related with the growth direction. In the XRD pattern of NWs-1, while the intensity of (002) peak is still high, the intensity of (111) peak is diminished and that of (400) peak increases significantly. The (002) and (400) peaks originate mainly from the planes parallel to the growth direction [010]. Since the nanowires are randomly oriented, the XRD would reflect mostly the separation of lattice planes lying along the growth direction but not much that of lattice planes perpendicular to the growth direction. For NWs-2 whose growth direction is random, the relative intensity is the same as that of the powder.

Raman scattering spectra of the β-Ga_2O_3 powder and nanowires are displayed in Figure 5. The peak position and relative intensity are consistent with those of the reported one.[24] It is noticeable that the peaks of NWs-1 show a redshift by an average value of 2 cm^{-1} from that of the powder. The peak width is slightly broader than that of the powder. In contrast, a blueshift can be found from the peaks of NWs-2, which is about 2 cm^{-1}. The redshift for NWs-1 is probably related with their defective crystalline structure.[21] The nearly defect-free structure of NWs-2 would result in the blueshift of the Raman peaks.

Figure 6 shows room temperature (300 K) PL spectrum obtained from two β-Ga_2O_3 nanowire samples. The excitation photon energy is 3.815 eV obtained from the 325-nm line of a He−Cd laser. Although the photon energy is below the band gap, a strong blue emission is observed. The NWs-1 exhibits a broad band centered at 415 nm. For NWs-2, the band center

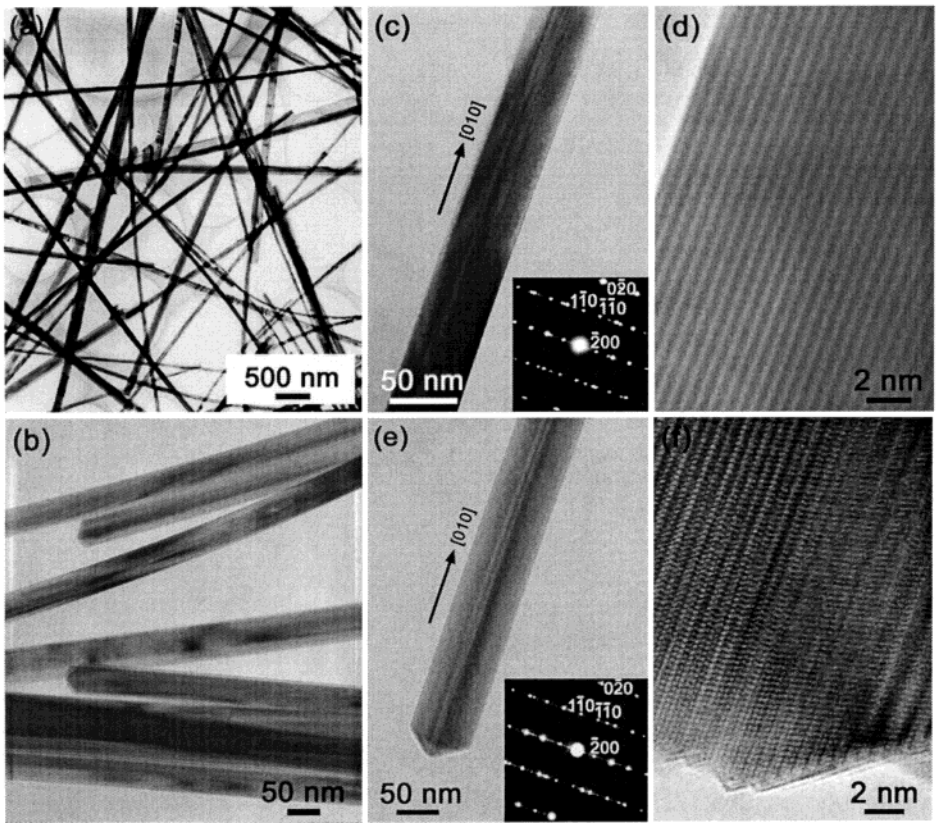

Figure 2. (a) TEM image showing the general morphology of the β-Ga_2O_3 nanowires grown without the catalyst (NWs-1). The diameter is uniformly 40−70 nm. (b) All nanowires have no amorphous outerlayers. (c) HRTEM image for a β-Ga_2O_3 nanowire with its corresponding SAED pattern (inset). (d) The distance between neighboring (200) planes parallel to the growth direction is about 5.94 Å. (e) HRTEM image for another β-Ga_2O_3 nanowire with its corresponding SAED (inset). (f) Atomic-resolved image for the sharp tip shows that the distance between neighboring (200) planes become shorter.

blueshifts to 380 nm and the bandwidth is narrower than that of NWs-1. The cathodoluminescence (CL, Gatan monoCL2) was performed at an acceleration voltage of 10 kV, showing a strong band only at this wavelength region. The present nanowires show the band center at the higher energy compared to the β-Ga_2O_3 single crystal (435 nm).[5] As for the PL mechanism, it was suggested that the blue luminescence originates from the recombination of an electron on a donor formed by oxygen vacancies and a hole on an acceptor formed by gallium vacancies.[25] Vasil'tsiv et al. proposed that the acceptor would be formed by a gallium−oxygen vacancy pair.[26] Binet and Courier suggested that a created hole on the acceptor would capture a created electron on the donor to form a trapped exciton, which recombines radiatively to emit a blue photon.[5] All these models explain the origin of the blue emission in terms of the defects. The NWs-1 probably possesses the more atomic vacancies because of the planar defect, compared to the NWs-2. The local energy of excitons trapped in the larger quantity of the atomic vacancies is usually decreased and distributed in the broader range, producing a broader redshifted emission. Therefore, the PL feature of the nanowires is consistent with the models described above. The present nanowires would contain less atomic vacancies than the reported single crystal, which can be a good candidate for the UV or blue emitter.

It is known that when Ga and Ga_2O_3 mixture is used, Ga_2O vapor is generated as follows: $4Ga(l) + Ga_2O_3(s) \rightarrow 3Ga_2O(g)$.[27,28] Without the catalyst, the reaction involving in the growth of the nanowires would be probably $Ga_2O(g) + O_2(g) \rightarrow Ga_2O_3(s)$. The growth would be categorized as vapor−solid (VS) mechanism, as suggested by other groups who did not use the catalyst.[11,16,18,20] When the Ni-deposited substrate is used, the Ga_2O vapor deposits on the Ni catalytic particles and dissolves into them, forming a miscible alloy. The continuous dissolving of Ga_2O and O_2 would lead the precipitation of $Ga_2O_3(s)$. Although the catalytic particles were not found, the growth would follow a vapor−liquid−solid (VLS) mechanism. The structure of the nanowires, including the growth direction and the degree of defects, depends strongly on the growth condition, particularly the catalyst. The result provides an excellent example for the role of catalyst that facilitates the growth of the nanowires by forming the liquid alloy. The catalyst increases the growth rate and also reduces the crystal defect. Since only [010] growth direction is available without catalyst, the [010] growth would be more kinetically favorable than the others. As the growth becomes efficient because of the catalyst, all growth direction may be permitted under our growth condition. The other works on the synthesis of β-Ga_2O_3 nanowires using the catalysts reported the different growth direction, for example, [001], [111], [200], [$\bar{1}$30], and so forth.[8,9,12,13,15] In contrast, the syntheses using no catalyst produced the [010] growth direction of β-Ga_2O_3 nanowires.[10,11,16,17] Those results are consistent with our present work, which would rationalize the catalytic effect on the growth of β-Ga_2O_3 nanowires.

4. Conclusion

In summary, we synthesized high-density β-Ga_2O_3 nanowires via thermal CVD using the reaction of Ga/Ga_2O_3 and O_2 at 1000−1200 °C. The CVD takes place without and with the catalyst (Ni nanoparticles). The diameter of nanowires is 30−80 nm with an average value of 50 nm. The length of nanowires

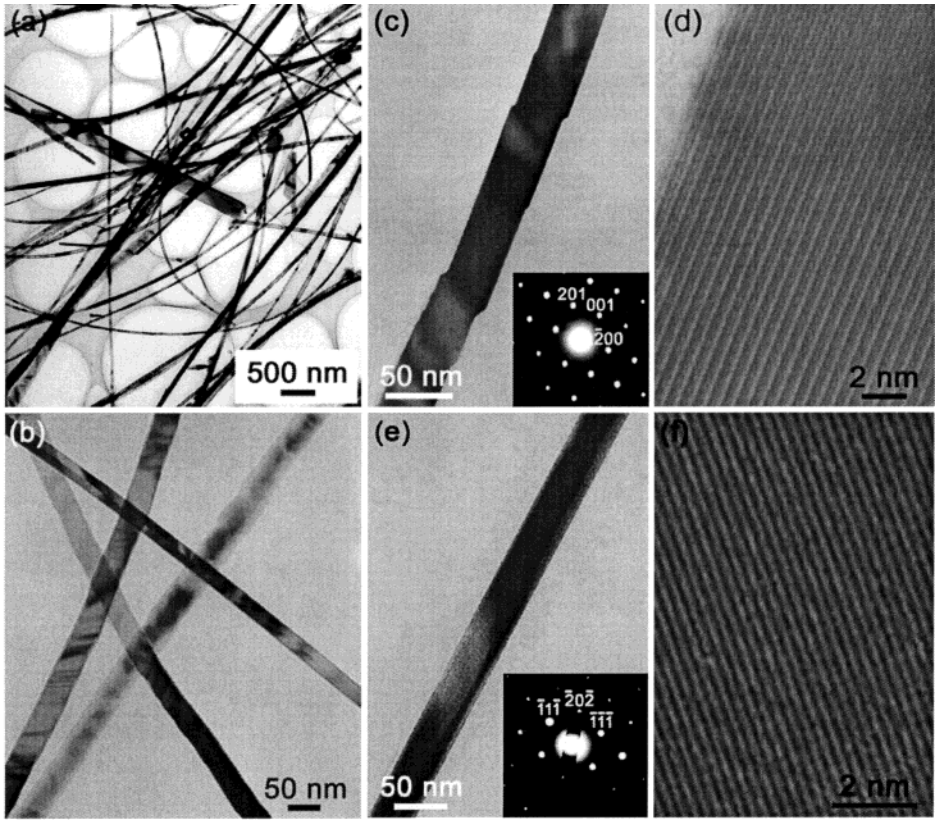

Figure 3. (a) TEM image showing the general morphology of the β-Ga_2O_3 nanowires grown with the Ni catalyst (NWs-2). The diameter is 30−80 nm and its average value is 50 nm. (b) It reveals no amorphous outerlayers. (c) HRTEM image for a β-Ga_2O_3 nanowire with its corresponding SAED pattern (inset). (d) The distance between neighboring (200) planes parallel to the growth direction is about 5.94 Å. (e) HRTEM image for another Ga_2O_3 nanowire with its corresponding SAED pattern (inset). The growth direction is tilted to the $[\bar{2}0\bar{2}]$ by 15°. (f) The neighboring (111) planes are well separated with a distance of 2.51 Å.

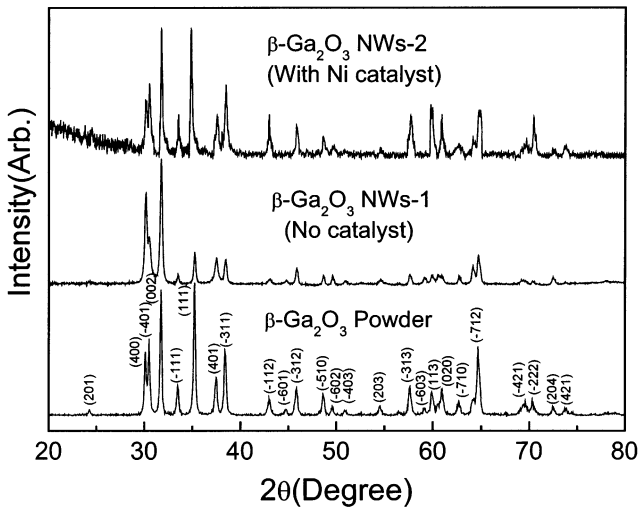

Figure 4. XRD patterns taken from the β-Ga_2O_3 powder and nanowires grown without (NWs-1) and with the Ni catalyst (NWs-2).

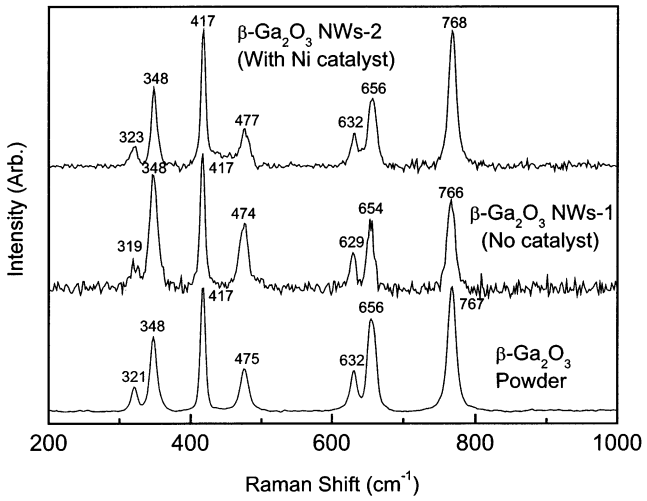

Figure 5. Raman spectrum for the β-Ga_2O_3 powder and nanowires grown without (NWs-1) and with the Ni catalyst (NWs-2).

grown without the catalyst (10−20 μm) is shorter than that grown with the Ni catalyst (up to 500 μm). HRTEM images and SAED pattern analysis reveal that the nanowires consist of single-crystalline monoclinic crystal. The nanowires grown without the catalyst (NWs-1) have uniformly the [010] growth direction. In contrast, the nanowires grown with the catalyst (NWs-2) are grown with random growth direction. The NWs-1 contains significant planar defects perpendicular to the growth direction, but the NWs-2 have the nearly defect-free crystalline structure. The relative peak intensity of the XRD pattern confirms the growth direction of β-Ga_2O_3 nanowires. The redshift of Raman peaks would be related with the defects of the nanowires. The room-temperature PL was measured using the 325-nm line of an argon ion laser, exhibiting a strong blue emission centered at 415 and 380 nm, respectively, for NWs-1 and NWs-2. The bandwidth is narrower for NWs-2, compared to that of NWs-1. The peak shift and broadening suggest that the emission would originate from the defect of the nanowires. The growth of NWs-1 and NWs-2 would follow the VS and VLS mechanisms, respectively. The catalyst would facilitate the growth of the nanowires, resulting in a less defect and random growth direction.

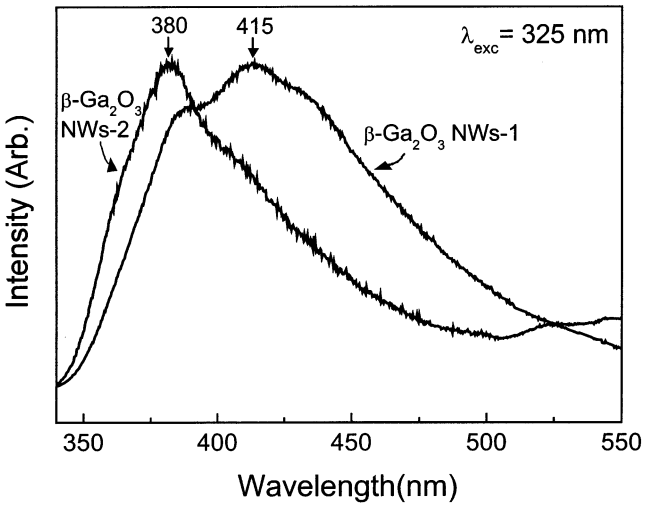

Figure 6. PL spectrum of the β-Ga_2O_3 nanowires grown without (NWs-1) and with the Ni catalyst (NWs-2). The excitation wavelength is the 325-nm line of argon laser.

Acknowledgment. National R&D Project for Nano Science and Technology supported the present work. SEM and X-ray diffraction analyses were performed at Basic Science Research Center in Seoul.

References and Notes

(1) Passlack, M.; Schubert, E. F.; Hobson, W. S.; Hong, M.; Moriya, N.; Chu, S. N. G.; Konstadinidis, K.; Mannaerts, J. P.; Schnoes, M. L.; Zydzik, G. J. *J. Appl. Phys*. **1995**, *77*, 686.

(2) Edwards, D. D.; Mason, T. O.; Goutenoire, F.; Poeppelmeier, K. R. *Appl. Phys. Lett.* **1997**, *70*, 1706.

(3) Ueda, N.; Hosono, H.; Waseda, R.; Kawazoe, H. *Appl. Phys. Lett.* **1997**, *70*, 3561.

(4) Hajnal, Z.; Miró, J.; Kiss, G.; Réti, F.; Deák, P.; Herndon, R. C.; Kuperberg, J. M. *J. Appl. Phys.* **1999**, *86*, 3792.

(5) Binet, L.; Gourier, D. *J. Phys. Chem. Solids* **1998**, *59*, 1241.

(6) Ogita, M.; Saika, N.; Nakanishi, Y.; Hatanaka, Y. *Appl. Surf. Sci.* **1999**, *142*, 188.

(7) Pohle, R.; Fleischer, M.; Meixner, H. *Sens. Actuators, B* **2000**, *68*, 151.

(8) Han, W. Q.; Kohler-Redlich, P.; Ernst, F.; Rühle, M. *Solid State Commun.* **2000**, *115*, 527.

(9) Choi, Y. C.; Kim, W. S.; Park, Y. S.; Lee, S. M.; Bae, D. J.; Lee, Y. H.; Park, G.; Choi, W. B.; Lee, N. S.; Kim, J. M. *Adv. Mater.* **2000**, *12*, 746.

(10) Hu, J. Q.; Li, Q.; Meng, X. M.; Lee, C. S.; Lee, S. T. *J. Phys. Chem. B* **2002**, *106*, 9536.

(11) Zhang, H. Z.; Kong, Y. C.; Wang, Y. Z.; Du, X.; Bai, Z. G.; Wang, J. J.; Yu, D. P.; Ding, Y.; Hang, Q. L.; Feng, S. Q. *Solid State Commun.* **1999**, *109*, 677.

(12) Li, J. Y.; Qiao, Z. Y.; Chen, X. L.; Chen, L.; Cao, Y. G.; He, M.; Li, H.; Cao, Z. M.; Zhang, Z. *J. Alloys Compd.* **2000**, *306*, 300.

(13) Li, J.; Chen, X.; Qiao, Z.; He, M.; Li, H. *J. Phys.: Condens. Matter* **2001**, *13*, L937.

(14) Sharma, S.; Sunkara, M. K. *J. Am. Chem. Soc.* **2002**, *124*, 12288.

(15) Liang, C. H.; Meng, G. W.; Wang, G. Z.; Wang, Y. W.; Zhang, L. D.; Zhang, S. Y. *Appl. Phys. Lett.* **2001**, *78*, 3202.

(16) Kim, B. C.; Sun, K. T.; Park, K. S.; Im, K. J.; Noh, T.; Sung, M. Y.; Kim, S.; Nahm, S.; Choi, Y. N.; Park, S. S. *Appl. Phys. Lett.* **2002**, *80*, 479.

(17) Dai, Z. R.; Pan, Z. W.; Wang, Z. L. *J. Phys. Chem. B* **2002**, *106*, 902.

(18) Wu, X. C.; Song, W. H.; Huang, W. D.; Pu, M. H.; Zhao, B.; Sun, Y. P.; Du, J. J. *Chem. Phys. Lett.* **2000**, *328*, 5.

(19) Li, Z. J.; Li, H. J.; Chen, X. L.; Li, L.; Xu, Y. P.; Li, K. Z. *J. Alloys Compd.* **2002**, *345*, 275.

(20) Zhang, J.; Zhang, L. *Solid State Commun.* **2002**, *122*, 493.

(21) Gao, Y. H.; Bando, Y.; Sato, T.; Zhang, Y. F.; Gao, X. Q. *Appl. Phys. Lett.* **2002**, *81*, 2267.

(22) Gundiah, G.; Govindaraj, A.; Rao, C. N. R. *Chem. Phys. Lett.* **2002**, *351*, 189.

(23) Ma, R.; Bando, Y. *Chem. Phys. Lett.* **2003**, *367*, 219.

(24) Dohy, D.; Lucazeau, G.; Revcolevschi, A. *J. Solid State Chem.* **1982**, *45*, 180.

(25) Harwig, T.; Kellendonk, F. *J. Solid Sate Chem.* **1978**, *24*, 255.

(26) Vasil'tsiv, V. I.; Zakharko, Ya. M.; Prim, Ya. I. *Ukr. Fiz. Zh.* **1988**, *33*, 1320.

(27) Frosch, C. J.; Thurmond, C. D. *J. Phys. Chem.* **1958**, *62*, 611.

(28) Frosch, C. J.; Thurmond, C. D. *J. Phys. Chem.* **1962**, *66*, 877.